



**HAL**  
open science

# Charge collective modes in correlated electron systems: Plasmons beyond the random phase approximation

Loïc Philoxene, Vu Hung Dao, Raymond Frésard

► **To cite this version:**

Loïc Philoxene, Vu Hung Dao, Raymond Frésard. Charge collective modes in correlated electron systems: Plasmons beyond the random phase approximation. 2024. hal-04710076

**HAL Id: hal-04710076**

**<https://hal.science/hal-04710076v1>**

Preprint submitted on 26 Sep 2024

**HAL** is a multi-disciplinary open access archive for the deposit and dissemination of scientific research documents, whether they are published or not. The documents may come from teaching and research institutions in France or abroad, or from public or private research centers.

L'archive ouverte pluridisciplinaire **HAL**, est destinée au dépôt et à la diffusion de documents scientifiques de niveau recherche, publiés ou non, émanant des établissements d'enseignement et de recherche français ou étrangers, des laboratoires publics ou privés.

# Charge Collective Modes in Correlated Electron Systems: Plasmons Beyond the Random Phase Approximation

Loïc Philoxene, Vu Hung Dao, and Raymond Frésard\*

Normandie Université, ENSICAEN, UNICAEN, CNRS, CRISMAT, 14000 Caen, France

(Dated: September 6, 2024)

Elucidating the impact of strong electronic interactions on the collective excitations of metallic systems has been of longstanding interest, mainly due to the inadequacy of the random phase approximation (RPA) in the strongly correlated regime. Here, we adopt our newly developed radial Kotliar and Ruckenstein slave boson representation to analyze the charge excitation spectrum of a Hubbard model, extended with long range interactions. Working on the face centered cubic lattice, at half filling, and in different coupling regimes ranging from uncorrelated to the metal-to-insulator transition, we compare our results to conventional RPA as a benchmark. We focus on the influence of the local and long range couplings on the particle-hole excitation continuum and the plasmon and upper Hubbard band collective modes. Beyond the weak coupling regime, we find numerous quantitative and even qualitative discrepancies between our method and standard RPA. Our work thus deepens the understanding of charge collective modes in correlated systems, and lays the foundations for future studies of a broad series of materials.

*Introduction.*— In their seminal series of papers, Pines and Bohm pioneered the study of collective modes arising in dynamical autocorrelation functions of the electron gas by introducing the random phase approximation (RPA) [1–3]. Focusing on density fluctuations, they argued that their spectra may be split into two components: i) an incoherent one associated with the random thermal motion of the individual electrons, and ii) a plasma oscillation mode. Having a classical analogue, the latter may be explained in simple terms, and is broadly documented [4–6]. Nevertheless, quantum corrections to this classical picture were recently addressed [7]. Furthermore, a series of applications backing on its existence have been put forward, ranging from nanophotonics [8–21], to energy conversion [22–26], and even cancer treatment [27–31].

Since its introduction, it has been established that the RPA remains sensible in the weak coupling regime only, and that it becomes unreliable as soon as the coupling strength becomes intermediate. Nevertheless, it may still be applied as a flexible tool in the thermodynamic limit, and it indeed remains broadly used, especially within quantum chemistry codes [32–34]. Besides, a series of calculations on model systems demonstrated qualitative failures of the approximation, especially in the context of the celebrated one band Hubbard model. In fact, key quantum collective phenomena entailed by the model, for example signatures of the upper Hubbard band, are missing in the charge excitation spectra when computed within the RPA. Multiple frameworks that try to overcome some of these shortcomings, and recover some of the missing features, have thus been proposed [35–40].

A broadly used approach to tackle correlated electrons is provided by Kotliar and Ruckenstein’s slave boson (KRSB) representation. This versatile tool may be applied to a series of microscopic models, such as the Hub-

bard model [41] and its extensions [42–44]. It consists in introducing a doublet of pseudofermions, along with four bosons, that generate the Fock space on each lattice site. In the functional integral formulation, this results in a Lagrangian that is bi-linear in the fermionic fields, although no Hubbard-Stratonovich decoupling is performed, thereby allowing for a description of electronic interactions at arbitrary coupling strengths. The reliability of the KRSB representation to the Hubbard model and its extensions has already been extensively discussed (see, e.g., Paragraph II.C.1 in Ref. [45] and references therein). A recent study also put forward quantitative agreement between the charge and spin structure factors computed in KRSB and resonant inelastic x-ray scattering data in electron-doped cuprates [44]. Within this representation, calculations are amenable to the thermodynamic limit as well, especially regarding the Mott metal-to-insulator transition [46] (MIT), and does not suffer from a weak coupling limitation. The resulting low energy spectra qualitatively differ from the RPA results, however [47]. They generically comprise a continuum, a zero-sound collective mode lying slightly above this continuum, and a signature of the upper Hubbard band in the form of a mode that disperses about  $\omega \sim U$  in the strong coupling regime. Below, we refer to the latter as the upper Hubbard band mode. This mode may, in the intermediate coupling regime, hybridize with the zero-sound one [47].

In the past twenty years, the extended Hubbard model, entailing non-local density-density interactions, has seen an upsurge of interest [45, 48–57] (see also [58] and references therein for a better overview). It has also been studied early on within the KRSB representation, and phase diagrams have been computed [42]. Below, we apply the radial gauge of the KRSB representation [59], in which the non-local interaction arises in a bi-linear form in terms of the boson fields. It allows for a systematic evaluation of long range correlations between density fluctuations. This formalism has recently been revisited

\* raymond.fresard@ensicaen.fr

and validated through exact calculations [60, 61].

The purpose of the present Letter is to compute the experimentally accessible energy loss spectrum of the extended Hubbard model, via the calculation of the dynamical dielectric function, which itself depends on the charge autocorrelation function. Special focus is made on the interplay of the plasmon mode (driven by the non-local Coulomb interaction), the upper Hubbard band (driven by the local interaction), and the low energy particle-hole excitation continuum.

*Model and methods.*— The Hamiltonian for the Hubbard model, extended by a long range Coulomb interaction, may be written as

$$\mathcal{H} = \sum_{i \neq j, \sigma} t_{ij} (c_{\sigma,i}^\dagger c_{\sigma,j} + \text{h.c.}) + U \sum_i n_{\uparrow,i} n_{\downarrow,i} + \frac{1}{2} \sum_{i \neq j} V_{ij} \left( 2 - \sum_{\sigma} n_{\sigma,i} \right) \left( 2 - \sum_{\sigma} n_{\sigma,j} \right), \quad (1)$$

where  $c_{i,\sigma}$  ( $\sigma = \uparrow, \downarrow$ ) is the canonical electron annihilation operator,  $n_{i,\sigma}$  is the associated electron number operator,  $t_{ij} = -t$  if  $i$  and  $j$  are nearest neighbors, and  $t_{ij} = 0$  otherwise, and we set  $\hbar = 1$  here and throughout. Here,  $t$  is the hopping amplitude,  $U$  is the Hubbard coupling, and  $V_{ij} = Va/|\mathbf{r}_i - \mathbf{r}_j|$  is the non-local Coulomb interaction, where  $a$  is the lattice spacing, and  $V$  is an effective coupling parameter. In the last term, the long range interaction has been chosen to couple to the hole densities  $2 - n$  for later convenience. It is, however, equivalent to the representation in terms of electron densities  $n$ , as they differ by an overall shift in energy, only.

We work in the grand canonical ensemble, and employ the radial gauge of the KRSB representation. In this paragraph, we give an outline of the formalism behind this radial KRSB representation, and refer to the Appendix A for a detailed derivation and technical discussions. In the original KRSB framework, one introduces a set of four auxiliary bosons  $e$ ,  $p_\sigma$ , and  $d$  (associated to unoccupied, singly occupied with spin projection  $\sigma$ , and doubly occupied atomic states, respectively), as well as a doublet of pseudofermions  $f_\sigma$  at each lattice site. Within the functional integral formalism, the canonical electron fields are mapped to a product of slave boson and pseudofermion fields as

$$c_{\sigma,i}(\tau) \rightarrow z_{\sigma,i}(\tau) f_{\sigma,i}(\tau), \quad (2)$$

where the fields  $z_{\sigma,i}(\tau)$  are functions of the boson fields (omitting the imaginary-time variable  $\tau$ ),

$$z_{\sigma,i} = e_i^* Y_{\sigma,i} p_{\sigma,i} + p_{-\sigma,i}^* Y_{\sigma,i} d_i, \quad (3)$$

where

$$Y_{\sigma,i} = [(e_i^* e_i + p_{-\sigma,i}^* p_{-\sigma,i})(1 - p_{-\sigma,i}^* p_{-\sigma,i} - e_i^* e_i)]^{-1/2}. \quad (4)$$

This representation is invariant under local  $U(1) \times U(1) \times U(1)$  gauge transformations, allowing

for the phase of three of the boson fields to be gauged away [62–64]. The boson fields deprived of their phase degree of freedom are coined radial slave bosons. Being real-valued, the radial slave boson fields are free from Bose condensation. Their expectation values are generically finite and can be well approximated in the thermodynamic limit via the saddle-point approximation. Corrections to the latter may be obtained when evaluating the Gaussian fluctuations [47], and the correspondence between this more precise evaluation and the time-dependent Gutzwiller approach [65] could recently be achieved—though by means of an extension in the formulation of the latter [66]. In the Cartesian gauge, the non-local interaction term reads  $\frac{1}{2} \sum_{i \neq j} V_{ij} (2 - p_{\uparrow,i}^2 - p_{\downarrow,i}^2 - 2d_i^* d_i) (2 - p_{\uparrow,j}^2 - p_{\downarrow,j}^2 - 2d_j^* d_j)$ . It is quartic in the bosonic fields, and can therefore not be integrated exactly. In contrast, in the radial gauge, one may re-write it as  $\frac{1}{2} \sum_{i \neq j} V_{ij} (2R_{e,i} + R_{\uparrow,i} + R_{\downarrow,i})(2R_{e,j} + R_{\uparrow,j} + R_{\downarrow,j})$ , after having made use of the constraints to eliminate the  $d$ -boson (see Appendix A and Ref. [61]). By doing so, both local and non-local interaction terms enter the action as quadratic terms in the radial slave bosons. Further details on the radial gauge are provided in Appendix A.

The charge excitation spectrum of the model can be analyzed through the evaluation of the loss function  $-\text{Im}[\varepsilon^{-1}(\mathbf{q}, \omega)]$ , which is experimentally accessible by electron energy loss spectroscopy or resonant inelastic x-ray scattering measurements.

To that end, we compute the inverse dielectric function as

$$\varepsilon^{-1}(q) = 1 - \left( \frac{U}{2} + V_{\mathbf{q}} \right) \chi_c(q), \quad (5)$$

where  $V_{\mathbf{q}} = 4\pi aV/|\mathbf{q}|^2$ ,  $q \equiv (\mathbf{q}, i\omega_n)$ ,  $\omega_n \equiv 2\pi n k_B T$ ,  $k_B$  is the Boltzmann constant, and  $T$  is the temperature. The density-density correlation function

$$\begin{aligned} \chi_c(q) &= \langle \delta n(-q) \delta n(q) \rangle \\ &= 4d^2 \langle \delta d'(-q) \delta d'(q) \rangle - 2d \langle \delta d'(-q) \delta R_e(q) \rangle \\ &\quad + \langle \delta R_e(-q) \delta R_e(q) \rangle, \end{aligned} \quad (6)$$

is calculated by taking into account Gaussian fluctuations of the boson fields around the paramagnetic saddle-point solution [47]. As detailed in the Appendix A, we obtain analytical expressions for  $\chi_c(q)$  and  $\varepsilon^{-1}(q)$ . The associated dynamical response functions are then evaluated on the real frequency axis with the substitution  $i\omega_n \rightarrow \omega + i0^+$ . The advantage of our procedure over numerical methods, lies in the obtained analytical expressions, which allow for an unambiguous analytical continuation, and can be physically interpreted in some limiting regimes.

The paramagnetic saddle-point of the KRSB representation has already been extensively studied in the literature [41–43, 47, 67]. In radial gauge, the study of the saddle-point remains identical.

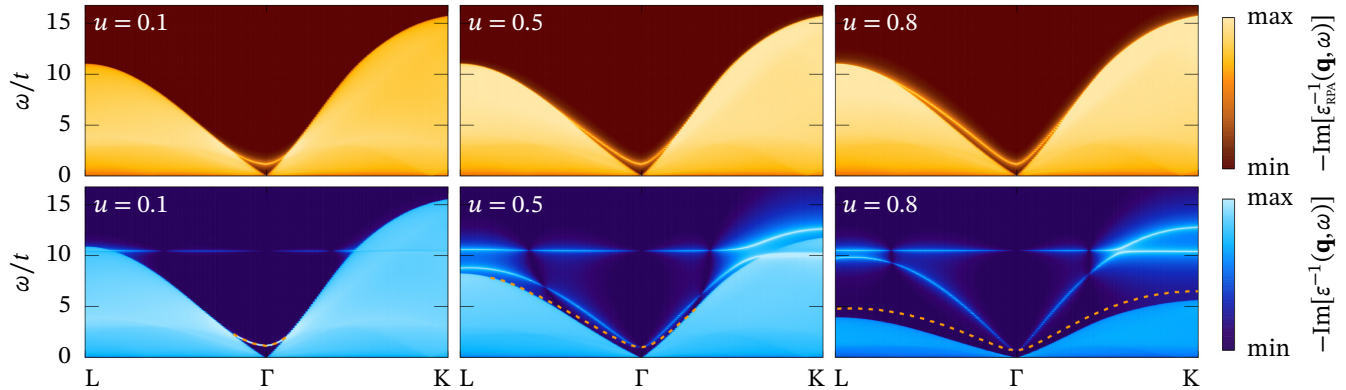


FIG. 1. Zero temperature RPA (top row) and radial KRSB (bottom row) energy loss spectra  $-\text{Im}[\varepsilon^{-1}(\mathbf{q}, \omega)]$ , in dependence on  $\mathbf{q}$  along  $L - \Gamma - K$ . Parameters:  $v = 0.1$  and  $u = 0.1, 0.5$ , and  $0.8$ , from left to right. The dashed lines in the bottom row denote the dispersion of the plasmon mode obtained by inserting the renormalized Lindhard function  $\Pi_0$  in the expression of the RPA dielectric function Eq. (7)

In this Letter, we focus on the face-centered-cubic (fcc) lattice as a representative example of three dimensional systems, since the simple cubic structure is scarcely realized. In this case, the bare dispersion is  $t_{\mathbf{k}} = -4t \left( \cos \frac{k_x}{2} \cos \frac{k_y}{2} + \cos \frac{k_y}{2} \cos \frac{k_z}{2} + \cos \frac{k_z}{2} \cos \frac{k_x}{2} \right)$ , where we set  $a = 1$ . As a proof of principle, we consider the half band-filling ( $n = 1$ ) case, which hosts the MIT, thereby allowing us to unravel the impact of strong electron correlations on the loss function. In this context, the critical coupling of the Mott transition is  $U_c = -8\xi_0$ , where  $\xi_0$  denotes the average bare kinetic energy. We find  $\xi_0 \simeq -0.16W$ , where  $W = 16t$  is the bare bandwidth. This yields  $U_c = 1.31W$ , which, due to the large coordination number of the fcc lattice, also compares favorably with the large coordination limit of dynamical mean-field theory (DMFT):  $U_c = 1.47W$  [68].

*Results.*— In the standard Hartree-Fock RPA (HF+RPA) framework, the density-density correlation function is computed as a series of particle-hole bubble diagrams for non-interacting electrons, linked with bare interaction vertices  $U/2 + V_{\mathbf{q}}$ . Under such approximations, the dynamical dielectric function reads [6]

$$\varepsilon_{\text{RPA}}(\mathbf{q}, \omega) = 1 + \left( \frac{U}{2} + V_{\mathbf{q}} \right) \Pi_0^{(0)}(\mathbf{q}, \omega), \quad (7)$$

where  $\Pi_0^{(0)}(\mathbf{q}, \omega)$  is the Lindhard function for the non-interacting system. Due to its perturbative essence, we cannot expect standard HF+RPA procedure to yield reasonable results in the strong coupling regime (see [47] and Appendix D for an assessment of some of the key features missing in the RPA treatment that are incorporated in the Cartesian and radial KRSB formalisms, respectively). However, we use it as a benchmark to highlight strong correlation effects when comparing it with the radial KRSB representation for values of  $U$  and/or

$V$  approaching  $U_c$ . In the following, we use the dimensionless coupling parameters  $u = U/U_c$  and  $v = V/U_c$ .

Let us now address representative examples of the energy loss spectra computed with Eq. (7) and with Eq. (5). We fix the value of  $v = 0.1$  and investigate values of  $u = 0.1, 0.5$ , and  $0.8$  at half filling and zero temperature. We also focus on values of  $\mathbf{q}$  along the representative symmetry lines  $L - \Gamma - K$ , with  $L = (\pi, \pi, \pi)$ ,  $\Gamma = (0, 0, 0)$ , and  $K = (\frac{3\pi}{2}, \frac{3\pi}{2}, 0)$ , for the wavevector dependence. On the face centered cubic lattice, the nearest neighbor distance is smallest (largest) along the  $\Gamma - K$  ( $\Gamma - L$ ) direction. The computed spectra are presented in Fig. 1. They generically comprise a low energy particle-hole excitation continuum. In RPA, this continuum is insensitive to the value of  $u$ , and it disperses from  $\omega(\Gamma) = 0$ , up to  $\omega(K) \simeq 16t$ . In our radial KRSB calculations, however, the continuum strongly depends on the value of  $u$ . Indeed, it is gradually narrowed by increasing the Hubbard coupling, with a maximum of its dispersion at  $\omega(K) \simeq 16t$  for  $u = 0.1$ , in contrast to  $\omega(K) \simeq 6t$ , only, for  $u = 0.8$ . This owes to the fact that the Lindhard function for the quasiparticles  $\Pi_0(\mathbf{q}, \omega)$  and the non-interacting Lindhard function  $\Pi_0^{(0)}(\mathbf{q}, \omega)$  are related via renormalization. For the considered paramagnetic phase, this reads (see Appendix B for a discussion)

$$\Pi_0^{(0)}(\mathbf{q}, \omega) = z_0^2 \Pi_0(\mathbf{q}, z_0^2 \omega), \quad (8)$$

where,  $z_0^2 = \langle z_{\sigma,i}^\dagger z_{\sigma,i} \rangle$  is the inverse mass renormalization factor, appearing as  $z_0^2 t_{\mathbf{k}}$  in the dispersion relation of the quasiparticles. One may thus explicitly see the decrease of the continuum's bandwidth, as the quasiparticle residue  $z_0^2 = 1 - u^2$  approaches zero when  $u$  approaches unity [47].

The RPA response features a single collective mode: the plasmon, which establishes at large wavelengths, above the continuum. When increasing  $\mathbf{q}$ , it enters the

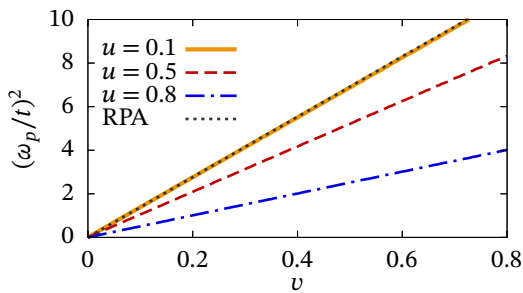


FIG. 2. Square of the plasma frequency  $\omega_p^2$  in dependence on the strength of the effective Coulomb coupling  $v$ . Parameters:  $u = 0.1, 0.5$ , and  $0.8$ . The plasma frequency obtained in standard RPA is also shown.

particle-hole continuum, and thus quickly becomes suppressed by Landau damping. For larger values of  $u$ , the mode gets overdamped at larger energy and wavevector, especially in the  $L$  direction, along which it disperses more. Its gap at  $\mathbf{q} = \Gamma$ , the plasma frequency  $\omega_p$ , remains unchanged and in fact depends on  $v$ , only. This can be understood from the expression

$$\omega_p \simeq \sqrt{-\frac{V\xi_0}{6}}, \quad (9)$$

obtained by a large wavelength expansion of the RPA dielectric function (derived in Appendix A). For  $v = 0.1$  (i.e.  $V = 2.1t$ ), this yields  $\omega_p \simeq t$ , which coincides with the gap shown in the top row of Fig. 1. Furthermore, we note that the plasma frequency computed with this expression does not depend on the value of  $u$ . In fact,  $u$  first enters the dispersion of the plasmon mode as a contribution of order  $|\mathbf{q}|^2$ . This additionally corroborates the observation that the plasmon mode disperses more for larger values of the Hubbard coupling. In the bottom row of Fig. 1, we see that the radial KRSB spectra possess two well-defined collective modes. Firstly, we observe the plasmon mode, similarly to the RPA. At weak coupling  $u = 0.1$ , the plasmon collective mode is also present at large wavelengths, only, as it enters the particle-hole continuum at approximately the same values of  $\mathbf{q}$  and  $\omega$  as in RPA. At larger couplings  $u = 0.5$  and  $0.8$ , though, the renormalization of the particle-hole continuum, along with the greater dispersion of the plasmon mode induced by  $u$ , allows for the latter to remain well-defined in a broader range of wavelengths. One also sees that the plasmon mode obtained by inserting the renormalized polarizability Eq. (8) in the RPA formula for the dielectric function correctly accounts for the value of the plasma frequency at arbitrary coupling. At finite wavelengths, however, this naive attempt to account for strong correlations within the RPA response noticeably deviates from the KRSB plasmon. Secondly, an additional collective mode establishes in the radial KRSB spectra. This mode, with a much larger gap at  $\Gamma$  of about  $\omega_{\text{UHB}} \simeq 10t$  for every values of  $u$ , corresponds to the aforementioned upper Hubbard band mode. Similarly to the plasmon

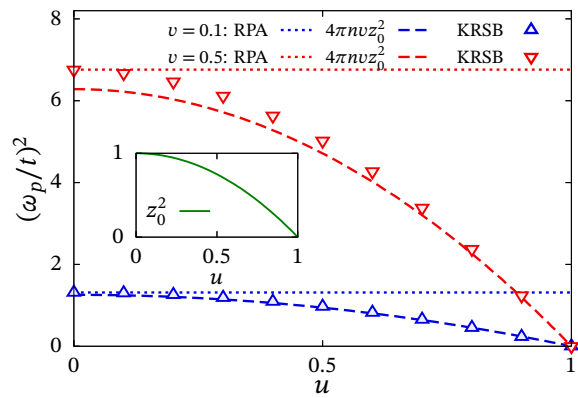


FIG. 3. Square of the radial KRSB plasma frequency  $\omega_p^2$  in dependence on the local coupling  $u$ . The RPA results, and the plasma frequency obtained by using the classical expression (see text) with  $m^* = 1/z_0^2$ , are also shown. Inset: Quasiparticle residue  $z_0^2$  in dependence on  $u$ . Parameters:  $v = 0.1$  and  $0.5$ .

mode, at weak coupling, it enters the particle-hole continuum at finite  $\mathbf{q}$ , inside which it quickly decays via Landau damping. It, however, disperses much less than the plasmon mode, with a bandwidth of at most one for  $u = 0.8$ .

In this two-modes picture, one might expect a level-crossing at finite  $\mathbf{q}$  between the two branches, at a given point of the parameter space. Yet, no point of exact degeneracy could be found, but either no-crossing or anticrossings between both modes, as depicted in the center and right panels of the bottom row in Fig. 1. Nonetheless, we observe multiple anticrossings with near-degeneracy, as can be seen for example close to  $K/2$  and energies around  $\omega \simeq 10t$  for  $u = 0.8$ . Close to these anticrossings, the upper Hubbard band mode and the plasmon mode strongly hybridize, and the excitations share both characters.

Fig. 2 presents the  $v$  dependence of the radial KRSB plasma frequency squared  $\omega_p^2$ , for values of  $u = 0.1, 0.5$ , and  $0.8$ . The RPA result is also shown for comparison, and one can see that in the weak coupling regime, the radial KRSB formalism correctly reproduces the RPA plasma frequency, as expected. Another expected property of the square of the plasma frequency is that it should scale with  $v$ , as we have  $\omega_p^2 \simeq 9.2v$  at weak coupling, which is also realized. However, the deviation of the plasma frequency from this analytical expression is seen to increase with  $u$ . This indicates that strong correlation effects, arising when the local coupling becomes sufficiently large, cause a softening of the plasmon mode, by opposition to the RPA picture in which the plasmon mode is barely affected.

The  $u$  dependence of the radial KRSB plasma frequency squared is shown in Fig. 3, for representative values of  $v = 0.1$  and  $0.5$ . The (constant) RPA result, for the same values of  $v$ , is also presented for comparison. We see that the plasma frequency decreases as the Hubbard cou-

pling increases, ranging from the RPA value for  $u = 0$ , to zero at the onset of the Mott transition. This can be qualitatively understood by considering the classical expression for the plasma frequency,  $\omega_p = \sqrt{4\pi n e^2 / m^*}$ , with  $n$  the electron density,  $e$  the electron charge, and  $m^*$  its effective mass. Recalling that, for an unscreened Coulomb interaction  $V = e^2$ , and that the band mass is given by the renormalization factor via  $z_0^2 t \sim 1/m^*$ , we see that the plasma frequency should decrease along with  $z_0^2$  when the Hubbard coupling is increased. This is better depicted in the inset of Fig. 3, in which  $\omega_p^2$  is shown as a function of the quasiparticle residue  $z_0^2$ . We clearly see that at the onset of the MIT, at which the effective mass diverges,  $\omega_p$  drops to zero. This vanishing of the plasma frequency at the onset of the Mott transition re-emphasizes the connection between the coherent and collective nature of the plasmon mode.

*Summary and conclusion.*— In summary, we have proposed a theoretical framework for the computation of charge excitation spectra in the presence of long range Coulomb interactions, and in the full range of correlation regimes. We evidenced quantitative and qualitative discrepancies between our results and standard RPA. In particular, we emphasized the influence of strong local correlations on the plasmon collective mode, showing the possibility for the plasmon to propagate undamped in

broader ranges of wavelengths at strong coupling, and recovering the expected dependence of the plasma frequency on the renormalized mass of the electrons. At the onset of the Mott transition, we found the plasma frequency to vanish along with the quasiparticle residue. Regions of strong hybridization between the plasmon and upper Hubbard band collective modes have also been unraveled. The benefits of the obtained analytical formula for the loss function are twofold. First, it allows for a straightforward analytical continuation, thereby yielding sharply defined collective modes. Second, simple approximations may be recovered in some limiting cases, providing easy access to physical quantities. As the computational cost is similar to that of standard RPA, our method, and possible future generalizations, may be employed to refine the incorporation of strong interactions in studies of correlated systems.

## ACKNOWLEDGMENTS

The authors gratefully thank Thilo Kopp for insightful discussions. This work was supported by Région Normandie through the ECOH project. Financial support provided by the ANR LISBON (ANR-20-CE05-0022-01) project is gratefully acknowledged.

## Appendix A: Derivation of the radial KRSB density autocorrelation function

### 1. Expression of the radial KRSB action functional

To circumvent the notorious failures of standard perturbation theory in interaction regimes where the coupling scale approaches the characteristic electrons hopping energy scale  $t$ , slave boson techniques introduce auxiliary fields in terms of which the interaction terms may be written as bilinear terms. In the context of the extended Hubbard model, a particular choice of such representation is that of Kotliar and Ruckenstein [41]. According to the exhaustive presentation provided in Ref. [61], the KRSB representation involves a doublet of fermionic fields  $\{f_{\uparrow,i}, f_{\downarrow,i}\}$ , together with four bosonic fields  $\{e_i, p_{\uparrow,i}, p_{\downarrow,i}, d_i\}$  (omitting the time variables), which are tied to empty, singly occupied (with spin projection  $\sigma \in \{\uparrow, \downarrow\}$ ), and doubly occupied lattice sites. In the radial gauge, the first three boson fields possess an amplitude degree of freedom, only, labeled  $R_{e,i}$  and  $R_{\sigma,i}$ . The grand canonical partition function then reads

$$\mathcal{Z} = \lim_{\nu \rightarrow 0} \lim_{N \rightarrow \infty} \lim_{\eta \rightarrow 0^+} \left[ \prod_{n=1}^N \prod_{i=1}^L \left( \int_{-\eta}^{\infty} dR_{e,i,n} dR_{\uparrow,i,n} dR_{\downarrow,i,n} \int_{-\infty}^{\infty} \frac{\epsilon d\alpha_{i,n}}{2\pi} \frac{\epsilon d\beta_{\uparrow,i,n}}{2\pi} \frac{\epsilon d\beta_{\downarrow,i,n}}{2\pi} \frac{dd'_{i,n} dd''_{i,n}}{\pi} \int \prod_{\sigma} df_{\sigma,i,n} df_{\sigma,i,n}^* \right) \times e^{-(\mathcal{S}_f[f^*, f, \psi] + \mathcal{S}_b[\psi])} \right], \quad (\text{A1})$$

where  $\epsilon = \beta/N$ , and the vector  $\psi = (R_e, d^*, d, R_{\uparrow}, R_{\downarrow}, \beta_{\uparrow}, \beta_{\downarrow}, \alpha)$  gathers the boson fields, as well as the time-dependent fields  $\alpha$  and  $\beta_{\sigma}$ . The latter are enforcing the constraints

$$R_{e,i} + R_{\uparrow,i} + R_{\downarrow,i} + d_i'^2 + d_i''^2 = 1, \quad (\text{A2})$$

$$R_{\sigma,i} + d_i'^2 + d_i''^2 = f_{\sigma,i}^* f_{\sigma,i}, \quad (\text{A3})$$

respectively. The action functional entails a purely bosonic contribution

$$\mathcal{S}_b[\psi] = \epsilon \sum_{n=1}^N \sum_{i=1}^L \left\{ \epsilon^{-1} d_{i,n}^* \left( d_{i,n} - e^{-\epsilon(U+i\tilde{\alpha}_{i,n}-i\beta_{\uparrow,i,n}-i\beta_{\downarrow,i,n})} d_{i,n-1} \right) + \frac{1}{2} \sum_{j \neq i} \sum_{\sigma, \sigma'} V_{ij} (R_{\sigma,i,n} + R_{e,i,n}) (R_{\sigma',j,n} + R_{e,j,n}) \right. \\ \left. + i\tilde{\alpha}_{i,n} (R_{e,i,n} + R_{\uparrow,i,n} + R_{\downarrow,i,n} - 1) - i \sum_{\sigma} \beta_{\sigma,i,n} R_{\sigma,i,n} \right\}, \quad (\text{A4})$$

and a mixed fermionic-bosonic contribution

$$\mathcal{S}_f[f^*, f, \psi] = \sum_{n=1}^N \sum_{i=1}^L \sum_{\sigma} f_{\sigma,i,n}^* \left( f_{\sigma,i,n} - e^{-\epsilon(i\beta_{\sigma,i,n}-\mu_0)} f_{\sigma,i,n-1} + \epsilon \sum_{j \neq i} \tilde{z}_{\sigma,i,n} z_{\sigma,j,n-1} t_{ij} f_{\sigma,j,n-1} \right). \quad (\text{A5})$$

Here,  $\tilde{\alpha}_{i,n} = \alpha_{i,n} - i\lambda_0$ , with some regulator  $\lambda_0 > 0$  ensuring convergence of the integrals, and where the notation  $\tilde{z}_{\sigma,i,n}$  has been introduced to stress that this field is not the complex conjugate of  $z_{\sigma,i,n}$ , but rather

$$z_{\sigma,i,n} = \frac{\sqrt{R_{e,i,n+1} R_{\sigma,i,n}} + \sqrt{R_{-\sigma,i,n+1}} d_{i,n}}{\sqrt{R_{e,i,n+1} + R_{-\sigma,i,n+1} - i\nu} \sqrt{1 - R_{e,i,n} - R_{-\sigma,i,n} + i\nu}}, \quad (\text{A6})$$

$$\tilde{z}_{\sigma,i,n} = \frac{\sqrt{R_{\sigma,i,n+1} R_{e,i,n}} + d_{i,n}^* \sqrt{R_{-\sigma,i,n}}}{\sqrt{1 - R_{e,i,n+1} - R_{-\sigma,i,n+1} - i\nu} \sqrt{R_{e,i,n} + R_{-\sigma,i,n} + i\nu}}. \quad (\text{A7})$$

Expanding the exponentials appearing in the action functional to leading order in  $\epsilon$ , and using the continuous imaginary-time notation, these expressions may conveniently be rewritten as

$$\mathcal{Z} = \int \mathcal{D}[f^*, f, \psi] e^{-(\mathcal{S}_f[f^*, f, \psi] + \mathcal{S}_b[\psi])}, \quad (\text{A8})$$

with

$$\mathcal{S}_b[\psi] = \int_0^{1/T} d\tau \sum_i \left[ U(d_i'^2 + d_i''^2) + \frac{1}{2} \sum_{j \neq i} \sum_{\sigma, \sigma'} V_{ij} (R_{\sigma,i} + R_{e,i}) (R_{\sigma',j} + R_{e,j}) \right. \\ \left. + i\alpha_i (R_{e,i} + d_i'^2 + d_i''^2 + R_{\uparrow,i} + R_{\downarrow,i} - 1) - i \sum_{\sigma} \beta_{\sigma,i} (R_{\sigma,i} + d_i'^2 + d_i''^2) + i(d_i' \partial_{\tau} d_i'' - d_i'' \partial_{\tau} d_i') \right], \quad (\text{A9})$$

and

$$\mathcal{S}_f[f^*, f, \psi] = \int_0^{1/T} d\tau \sum_{i,j} \sum_{\sigma} f_{\sigma,i}^* [(\partial_{\tau} - \mu_0 + i\beta_{\sigma,i}) \delta_{i,j} + z_{\sigma,i}^* z_{\sigma,j} t_{ij}] f_{\sigma,j}, \quad (\text{A10})$$

where the time labels  $\tau = \lim_{N \rightarrow \infty} \epsilon$  have been omitted for clarity, and  $d_i'$  and  $d_i''$  denote the real and imaginary parts of the  $d_i$  boson, respectively.

One could then demand proofs of the correctness of such a representation. In the presence of non-local interactions, this has been, most recently, provided by an explicit calculation of the partition function and correlation functions of the two-site cluster. Even though it acts as a toy integrable model, this limit of the extended Hubbard model has been shown to harbor all the technical hurdles of larger system sizes [61].

## 2. Expansion of the action functional around the paramagnetic saddle-point

### a. Paramagnetic saddle-point

At the paramagnetic saddle-point, the slave boson amplitudes take the expectation values

$$\psi^{\text{SP}} = (E, d, 0, P, P, \beta_0, \beta_0, \alpha), \quad (\text{A11})$$

the values of which are determined in dependence on the model parameters by solving the saddle-point equation [41–43, 47, 63, 69]

$$\frac{(1-x^2)x^4}{x^4-\delta^2} = \frac{U}{U_0}, \quad (\text{A12})$$

where  $\delta = 1 - n$  is the hole doping in a half-filled band, and  $U_0$  is a coupling scale which, at half filling ( $\delta = 0$ ), corresponds to the critical coupling of the interaction-driven Mott transition. At arbitrary doping,  $U_0$  reads

$$U_0 = -\frac{8\xi_0}{1-\delta^2}, \quad (\text{A13})$$

with the semi-renormalized kinetic energy

$$\xi_0 = \frac{2}{L} \sum_{\mathbf{k}} n_F(E_{\mathbf{k}}) t_{\mathbf{k}}, \quad (\text{A14})$$

where

$$t_{\mathbf{k}} = -4t \left( \cos \frac{k_x}{2} \cos \frac{k_y}{2} + \cos \frac{k_y}{2} \cos \frac{k_z}{2} + \cos \frac{k_z}{2} \cos \frac{k_x}{2} \right), \quad (\text{A15})$$

is the bare dispersion of the fcc lattice, and

$$E_{\mathbf{k}} = z_0^2 t_{\mathbf{k}} - (\mu - \beta_0), \quad (\text{A16})$$

is the quasiparticle dispersion, where  $z_0 = \langle z_{\sigma,i} \rangle$ . Note that the value of  $V$  does not enter Eq. (A12), hence the saddle-point values of the  $e$ ,  $p_\sigma$ , and  $d$  slave boson amplitudes do not depend on  $V$ . It turns out that the effect of  $V$  is simply to induce a shift in the values of the saddle-point amplitudes of  $\alpha$  and  $\beta_0$

$$\alpha|_V = \alpha|_{V=0} - 2(2-n)V_0, \quad (\text{A17})$$

$$\beta_0|_V = \beta_0|_{V=0} - (2-n)V_0, \quad (\text{A18})$$

that nevertheless leaves Eq. (A12) unaffected. Here,  $V_0 = V_{\mathbf{q}=\Gamma}$ .

### b. Gaussian fluctuations around the saddle-point

In order to investigate the excitations of the paramagnetic ground state of the system, we begin by expanding the action functional to second order in the field fluctuations

$$\delta\psi_{\mu,i}(\tau) = \psi_{\mu,i}(\tau) - \psi_{\mu}^{\text{SP}}, \quad (\text{A19})$$

about the paramagnetic saddle-point. This procedure yields contributions of increasing order in the field fluctuations, from which we only retain the zero-th to second orders,

$$\mathcal{S}[f^*, f, \psi] \simeq \mathcal{S}^{(0)}[f^*, f] + \mathcal{S}^{(1)}[f^*, f, \delta\psi] + \mathcal{S}^{(2)}[f^*, f, \delta\psi]. \quad (\text{A20})$$

Once again, we split the different orders of the contributions in bosonic  $\mathcal{S}_b$  and mixed  $\mathcal{S}_f$  sectors. The bosonic sector then contains the contributions

$$\mathcal{S}_b^{(0)} = \frac{L}{T} \left[ U d^2 + \frac{1}{2} V_0 (2-n)^2 - 2\beta_0 (P + d^2) + \alpha (E + 2P + d^2 - 1) \right], \quad (\text{A21})$$

$$\begin{aligned} \mathcal{S}_b^{(1)}[\delta\psi] = \sqrt{\frac{L}{T}} \left\{ [\alpha + 2V_0(2-n)] \delta R_e(0) + 2d[\alpha - 2\beta_0 + U] \delta d'(0) + [\alpha - \beta_0 + V_0(2-n)] \sum_{\sigma} \delta R_{\sigma}(0) \right. \\ \left. - (P + d^2) \sum_{\sigma} \delta \beta_{\sigma}(0) + (E + 2P + d^2 - 1) \delta \alpha(0) \right\}, \quad (\text{A22}) \end{aligned}$$



$$\mathcal{S}_b^{(2)}[\delta\psi] = \sum_q \sum_{\mu,\nu} \delta\psi_\mu(-q) D_{b,\mu\nu}^{-1}(q) \delta\psi_\nu(q), \quad (\text{A23})$$

where  $L$  is the number of lattice sites,  $q = (\mathbf{q}, i\omega_n)$ , with  $\omega_n$  a bosonic (i.e. even) Matsubara frequency. We also introduced the  $8 \times 8$  matrix

$$\underline{D}_b^{-1}(q) = \begin{pmatrix} 2V_{\mathbf{q}} & 0 & 0 & V_{\mathbf{q}} & V_{\mathbf{q}} & 0 & 0 & \frac{1}{2} \\ 0 & \alpha - 2\beta_0 + U & \omega_n & 0 & 0 & -d & -d & d \\ 0 & -\omega_n & \alpha - 2\beta_0 + U & 0 & 0 & 0 & 0 & 0 \\ V_{\mathbf{q}} & 0 & 0 & \frac{1}{2}V_{\mathbf{q}} & \frac{1}{2}V_{\mathbf{q}} & -\frac{1}{2} & 0 & \frac{1}{2} \\ V_{\mathbf{q}} & 0 & 0 & \frac{1}{2}V_{\mathbf{q}} & \frac{1}{2}V_{\mathbf{q}} & 0 & -\frac{1}{2} & \frac{1}{2} \\ 0 & -d & 0 & -\frac{1}{2} & 0 & 0 & 0 & 0 \\ 0 & -d & 0 & 0 & -\frac{1}{2} & 0 & 0 & 0 \\ \frac{1}{2} & d & 0 & \frac{1}{2} & \frac{1}{2} & 0 & 0 & 0 \end{pmatrix}. \quad (\text{A24})$$

In the fermionic sector, we have to expand the  $z$ -factors in powers of the slave boson fluctuations,

$$\begin{aligned} z_{\sigma,i}(\tau) &\simeq z_0 + \sum_{\mu} \frac{\partial z_{\sigma,i}(\tau)}{\partial \psi_{\mu,i}(\tau)} \Big|_{\psi=\psi^{\text{SP}}} \delta\psi_{\mu,i}(\tau) + \frac{1}{2} \sum_{\mu,\nu} \frac{\partial^2 z_{\sigma,i}(\tau)}{\partial \psi_{\mu,i}(\tau) \partial \psi_{\nu,i}(\tau)} \Big|_{\psi=\psi^{\text{SP}}} \delta\psi_{\mu,i}(\tau) \delta\psi_{\nu,i}(\tau) \\ &= z_0 + \sum_{\mu} Z_{\sigma,\mu}^{(1)} \delta\psi_{\mu,i}(\tau) + \frac{1}{2} \sum_{\mu,\nu} Z_{\sigma,\mu\nu}^{(2)} \delta\psi_{\mu,i}(\tau) \delta\psi_{\nu,i}(\tau), \end{aligned} \quad (\text{A25})$$

where the derivatives of  $z_{\sigma}$  are denoted

$$Z_{\sigma,\mu}^{(1)} = \frac{\partial z_{\sigma,i}(\tau)}{\partial \psi_{\mu,i}(\tau)} \Big|_{\psi=\psi^{\text{SP}}}, \quad (\text{A26})$$

$$Z_{\sigma,\mu\nu}^{(2)} = \frac{\partial^2 z_{\sigma,i}(\tau)}{\partial \psi_{\mu,i}(\tau) \partial \psi_{\nu,i}(\tau)} \Big|_{\psi=\psi^{\text{SP}}}. \quad (\text{A27})$$

Doing so, we find that the contributions, up to second order in the slave boson fields fluctuations, sum up to

$$\mathcal{S}_f[f^*, f, \delta\psi] \simeq \sum_{\sigma} \sum_{k,k'} f_{\sigma}^*(k) [-G_0^{-1}(k, k') + H_{\sigma}(k, k')] f_{\sigma}(k'), \quad (\text{A28})$$

where  $k = (\mathbf{k}, i\omega_{\ell})$ , with  $\omega_{\ell}$  a fermionic Matsubara frequency, and

$$G_0^{-1}(k, k') = [i\omega_{\ell} + (\mu - \beta_0) - z_0^2 t_{\mathbf{k}}] \delta_{k,k'}, \quad (\text{A29})$$

$$\begin{aligned} H_{\sigma}(k, k') &= \sqrt{\frac{T}{L}} \left\{ \delta\beta_{\sigma}(k - k') + z_0 \sum_{\mu} [\bar{Z}_{\sigma,\mu}^{(1)} t_{\mathbf{k}'} + Z_{\sigma,\mu}^{(1)} t_{\mathbf{k}}] \delta\psi_{\mu}(k - k') \right\} \\ &+ \frac{T}{L} \sum_q \sum_{\mu,\nu} \delta\psi_{\mu}(k - k' - q) \left\{ \frac{z_0}{2} [\bar{Z}_{\sigma,\mu\nu}^{(2)} t_{\mathbf{k}'} + Z_{\sigma,\mu\nu}^{(2)} t_{\mathbf{k}}] + \bar{Z}_{\sigma,\mu}^{(1)} Z_{\sigma,\nu}^{(1)} t_{\mathbf{k}'+\mathbf{q}} \right\} \delta\psi_{\nu}(q), \end{aligned} \quad (\text{A30})$$

where  $\bar{Z}_{\sigma,\mu}^{(1)} = (Z_{\sigma,\mu}^{(1)})^*$ . Using the integration rules for Gaussian integrals over Grassmann fields, we explicitly integrate the partition function over the pseudofermions

$$\begin{aligned} \mathcal{Z}_f &= \exp \left\{ \sum_{\sigma} \text{tr} [\ln(-\underline{G}_0^{-1} + \underline{H}_{\sigma})] \right\} \\ &= \det(\underline{G}_0^{-1})^2 \exp \left\{ \sum_{\sigma} \text{tr} [\ln(\underline{\mathbb{1}} - \underline{G}_0 \underline{H}_{\sigma})] \right\} \\ &\simeq \det(\underline{G}_0^{-1})^2 \exp \left\{ - \sum_{\sigma} \text{tr} \left[ \underline{G}_0 \underline{H}_{\sigma} + \frac{1}{2} \underline{G}_0 \underline{H}_{\sigma} \underline{G}_0 \underline{H}_{\sigma} \right] \right\} \\ &= \det(\underline{G}_0^{-1})^2 \exp \left\{ - \sum_q \sum_{\mu,\nu} \delta\psi_{\mu}(-q) D_{f,\mu\nu}^{-1}(q) \delta\psi_{\nu}(q) \right\}, \end{aligned} \quad (\text{A31})$$

where the trace is taken over the wavevectors and Matsubara frequencies. For the first term, this yields

$$\begin{aligned}
\text{tr}(\underline{G}_0 \underline{H}_\sigma) &= \sum_{k_1, k_2} G_0(k_1, k_2) H_\sigma(k_2, k_1) \\
&= \sum_k G_0(k) H_\sigma(k, k) \\
&= \sum_k G_0(k) \left\{ \sqrt{\frac{T}{L}} \left[ \delta\beta_\sigma(0) + 2z_0 \sum_\mu \text{Re}(Z_{\sigma, \mu}^{(1)}) t_{\mathbf{k}} \delta\psi_\mu(0) \right] \right. \\
&\quad \left. + \frac{T}{L} \sum_q \sum_{\mu, \nu} \delta\psi_\mu(-q) \left[ z_0 \text{Re}(Z_{\sigma, \mu\nu}^{(2)}) t_{\mathbf{k}} + \bar{Z}_{\sigma, \mu}^{(1)} Z_{\sigma, \nu}^{(1)} t_{\mathbf{k}+\mathbf{q}} \right] \delta\psi_\nu(q) \right\}, \\
&= -\frac{1}{2} \sum_q \sum_{\mu, \nu} \delta\psi_\mu(-q) \left[ z_0 \text{Re}(Z_{\sigma, \mu\nu}^{(2)}) \xi_{\mathbf{0}} + \bar{Z}_{\sigma, \mu}^{(1)} Z_{\sigma, \nu}^{(1)} \xi_{\mathbf{q}} \right] \delta\psi_\nu(q). \tag{A32}
\end{aligned}$$

In the last line, we used the fact that the terms of first order in the fields fluctuations are compensated by the bosonic part at the saddle-point, and we defined

$$\xi_{\mathbf{q}} = -\frac{2T}{L} \sum_k G_0(k) t_{\mathbf{k}+\mathbf{q}} = \frac{2}{L} \sum_{\mathbf{k}} n_F(E_{\mathbf{k}}) t_{\mathbf{k}+\mathbf{q}}. \tag{A33}$$

For the second term, we have, to second order in the boson fields fluctuations,

$$\begin{aligned}
\text{tr}\left(\frac{1}{2} \underline{G}_0 \underline{H}_\sigma \underline{G}_0 \underline{H}_\sigma\right) &= \frac{1}{2} \sum_{k_1, \dots, k_4} G_0(k_1, k_2) H_\sigma(k_2, k_3) G_0(k_3, k_4) H_\sigma(k_4, k_1) \\
&= \frac{T}{2L} \sum_{k_1, k_2} G_0(k_1) G_0(k_2) \left\{ \delta\beta_\sigma(k_1 - k_2) \delta\beta_\sigma(k_2 - k_1) \right. \\
&\quad \left. + \delta\beta_\sigma(k_1 - k_2) z_0 \sum_\mu [\bar{Z}_{\sigma, \mu}^{(1)} t_{\mathbf{k}_1} + Z_{\sigma, \mu}^{(1)} t_{\mathbf{k}_2}] \delta\psi_\mu(k_2 - k_1) + \text{h.c.} \right. \\
&\quad \left. + \sum_{\mu, \nu} \delta\psi_\mu(k_1 - k_2) z_0^2 [\bar{Z}_{\sigma, \mu}^{(1)} t_{\mathbf{k}_2} + Z_{\sigma, \mu}^{(1)} t_{\mathbf{k}_1}] [\bar{Z}_{\sigma, \nu}^{(1)} t_{\mathbf{k}_1} + Z_{\sigma, \nu}^{(1)} t_{\mathbf{k}_2}] \delta\psi_\nu(k_2 - k_1) \right\} \\
&= \frac{T}{2L} \sum_q \sum_{\mu, \nu} \delta\psi_\mu(-q) \sum_k G_0(k) G_0(k+q) \left\{ (\delta_{\mu\nu, 66} \delta_{\sigma, \uparrow} + \delta_{\mu\nu, 77} \delta_{\sigma, \downarrow}) \right. \\
&\quad \left. + 2z_0 [\bar{Z}_{\sigma, \nu}^{(1)} t_{\mathbf{k}} + Z_{\sigma, \nu}^{(1)} t_{\mathbf{k}+\mathbf{q}}] (\delta_{\mu, 6} \delta_{\sigma, \uparrow} + \delta_{\mu, 7} \delta_{\sigma, \downarrow}) + \text{h.c.} \right. \\
&\quad \left. + z_0^2 [2\text{Re}(Z_{\sigma, \mu}^{(1)} Z_{\sigma, \nu}^{(1)}) t_{\mathbf{k}} t_{\mathbf{k}+\mathbf{q}} + \bar{Z}_{\sigma, \mu}^{(1)} Z_{\sigma, \nu}^{(1)} t_{\mathbf{k}+\mathbf{q}}^2 + Z_{\sigma, \mu}^{(1)} \bar{Z}_{\sigma, \nu}^{(1)} t_{\mathbf{k}}^2] \delta\psi_\nu(q) \right\} \\
&= -\frac{1}{2} \sum_q \sum_{\mu, \nu} \delta\psi_\mu(-q) \left\{ \frac{1}{2} X_{00}(q) (\delta_{\mu\nu, 66} \delta_{\sigma, \uparrow} + \delta_{\mu\nu, 77} \delta_{\sigma, \downarrow}) \right. \\
&\quad \left. + z_0 [\bar{Z}_{\sigma, \mu}^{(1)} X_{01}(q) + Z_{\sigma, \mu}^{(1)} X_{10}(q)] (\delta_{\mu, 6} \delta_{\sigma, \uparrow} + \delta_{\mu, 7} \delta_{\sigma, \downarrow}) + \text{h.c.} \right. \\
&\quad \left. + \frac{z_0^2}{2} [2\text{Re}(Z_{\sigma, \mu}^{(1)} Z_{\sigma, \nu}^{(1)}) X_{11}(q) + \bar{Z}_{\sigma, \mu}^{(1)} Z_{\sigma, \nu}^{(1)} X_{20}(q) + Z_{\sigma, \mu}^{(1)} \bar{Z}_{\sigma, \nu}^{(1)} X_{02}(q)] \delta\psi_\nu(q) \right\}, \tag{A34}
\end{aligned}$$

where we introduced

$$X_{mn}(q) = -\frac{2T}{L} \sum_k G_0(k) G_0(k+q) t_{\mathbf{k}}^m t_{\mathbf{k}+\mathbf{q}}^n. \tag{A35}$$

Using the fact that, at the paramagnetic saddle-point,

$$Z_{\sigma, \mu}^{(1)} = \bar{Z}_{\sigma, \mu}^{(1)} = Z_\mu^{(1)}, \quad \text{for } \mu \in \{1, 2, 4, 5\}, \tag{A36}$$

$$Z_{\uparrow, \mu}^{(1)} = Z_{\downarrow, \mu}^{(1)}, \quad \text{for } \mu \in \{1, 2, 3\}, \tag{A37}$$

$$\bar{Z}_{\sigma, 3}^{(1)} = -Z_{\sigma, 3}^{(1)}, \tag{A38}$$

$$\text{Re}(Z_{\sigma, \mu 3}^{(2)}) = 0, \quad \text{for } \mu \neq 3, \tag{A39}$$

for all  $\sigma \in \uparrow, \downarrow$ , we finally obtain the matrix elements of the fermionic sector of the inverse propagator

$$D_{f,\mu\nu}^{-1}(q) = D_{f,\nu\mu}^{-1}(q) = \frac{1}{2}z_0\xi_0 \sum_{\sigma} Z_{\sigma,\mu\nu}^{(2)} + \frac{1}{2} \sum_{\sigma} Z_{\sigma,\mu}^{(1)} Z_{\sigma,\nu}^{(1)} \left[ \xi_{\mathbf{q}} - \frac{1}{2}z_0^2\Pi_2(q) \right], \quad \text{for } \mu, \nu = 1, 2, 4, 5, \quad (\text{A40})$$

$$D_{f,\mu 3}^{-1}(q) = -D_{f,3\mu}^{-1}(q) = -\frac{i\omega_n}{4} \sum_{\sigma} Z_{\sigma,\mu}^{(1)} Z_{\sigma,3}^{(1)} \Pi_1(q), \quad \text{for } \mu = 1, 2, 4, 5, \quad (\text{A41})$$

$$D_{f,33}^{-1}(q) = z_0\xi_0 \frac{\partial^2 \text{Re}[z_{\sigma,i}(\tau)]}{\partial d_i''(\tau) \partial d_i''(\tau)} \Big|_{\psi=\psi^{\text{SP}}} + \left| \frac{\partial z_{\sigma,i}(\tau)}{\partial d_i''(\tau)} \right|_{\psi=\psi^{\text{SP}}}^2 \left[ \xi_0 + \frac{\omega_n^2}{2z_0^2} \Pi_0(q) \right], \quad (\text{A42})$$

$$D_{f,\mu 6}^{-1}(q) = D_{f,6\mu}^{-1}(q) = -\frac{1}{4}z_0 Z_{\uparrow,\mu} \Pi_1(q), \quad \text{for } \mu = 1, 2, 4, 5, \quad (\text{A43})$$

$$D_{f,\mu 7}^{-1}(q) = D_{f,7\mu}^{-1}(q) = -\frac{1}{4}z_0 Z_{\downarrow,\mu} \Pi_1(q), \quad \text{for } \mu = 1, 2, 4, 5, \quad (\text{A44})$$

$$D_{f,66}^{-1}(q) = D_{f,77}^{-1}(q) = -\frac{1}{4} \Pi_0(q), \quad (\text{A45})$$

$$D_{f,\mu 8}^{-1}(q) = D_{f,8\mu}^{-1}(q) = 0, \quad \text{for all } \mu, \quad (\text{A46})$$

where

$$\Pi_m(q) = -\frac{2T}{L} \sum_k G_0(k) G_0(k+q) (t_{\mathbf{k}} + t_{\mathbf{k}+\mathbf{q}})^m. \quad (\text{A47})$$

### c. Effective Gaussian theory for the slave boson fluctuations

With the above two contributions, we arrive at the effective action functional for the fluctuations of the slave boson fields

$$\mathcal{S}_{\text{eff}}[\delta\psi] = \sum_q \sum_{\mu,\nu} \delta\psi_{\mu}(-q) D_{\mu\nu}^{-1}(q) \delta\psi_{\nu}(q), \quad (\text{A48})$$

where the inverse propagator for the boson field fluctuations  $\underline{D}^{-1}(q) = \underline{D}_b^{-1}(q) + \underline{D}_f^{-1}(q)$ , is a  $8 \times 8$  matrix in the  $\delta\psi(q)$  basis. However, if we perform a unitary change of basis

$$\delta\psi'(q) = \{\delta R_e(q), \delta d'(q), \delta d''(q), \delta R_0(q), \delta\beta_0(q), \delta\alpha(q), \delta R_z(q), \delta\beta_z(q)\}, \quad (\text{A49})$$

where

$$\delta R_0(q) = \frac{1}{\sqrt{2}} [\delta R_{\uparrow}(q) + \delta R_{\downarrow}(q)], \quad (\text{A50})$$

$$\delta R_z(q) = \frac{1}{\sqrt{2}} [\delta R_{\uparrow}(q) - \delta R_{\downarrow}(q)], \quad (\text{A51})$$

$$\delta\beta_0(q) = \frac{1}{\sqrt{2}} [\delta\beta_{\uparrow}(q) + \delta\beta_{\downarrow}(q)], \quad (\text{A52})$$

$$\delta\beta_z(q) = \frac{1}{\sqrt{2}} [\delta\beta_{\uparrow}(q) - \delta\beta_{\downarrow}(q)], \quad (\text{A53})$$

we can decouple the inverse propagator into a pure charge fluctuations sector, with basis

$$\delta\psi_c(q) = \{\delta R_e(q), \delta d'(q), \delta d''(q), \delta R_0(q), \delta\beta_0(q), \delta\alpha(q)\}, \quad (\text{A54})$$

and a pure spin fluctuations sector, with basis

$$\delta\psi_s(q) = \{\delta R_z(q), \delta\beta_z(q)\}. \quad (\text{A55})$$

To simplify notation, in the following, we refer to the fields fluctuations using the base Eq. (A49), and drop the prime exponent. This means that the basis of the charge sector corresponds to  $\{\delta\psi_{\mu}(q)\}$ , for  $\mu = 1, \dots, 6$ , while the basis

of the spin sector corresponds to  $\mu = 7$  and 8. The matrix elements for the charge sector of the fluctuation matrix then read

$$D_{11}^{-1}(q) = 2V_{\mathbf{q}} + D_{f,11}^{-1}(q), \quad (\text{A56})$$

$$D_{12}^{-1}(q) = D_{21}^{-1}(q) = D_{f,12}^{-1}(q), \quad (\text{A57})$$

$$D_{13}^{-1}(q) = -D_{13}^{-1}(q) = -\frac{i\omega_n}{2}\Pi_1(q)Z_1^{(1)}Z_3^{(1)}, \quad (\text{A58})$$

$$D_{14}^{-1}(q) = D_{41}^{-1}(q) = \sqrt{2}V_{\mathbf{q}} + D_{f,14}^{-1}(q), \quad (\text{A59})$$

$$D_{15}^{-1}(q) = D_{51}^{-1}(q) = -\frac{1}{2\sqrt{2}}z_0Z_1^{(1)}\Pi_1(q), \quad (\text{A60})$$

$$D_{16}^{-1}(q) = D_{61}^{-1}(q) = \frac{1}{2}, \quad (\text{A61})$$

$$D_{22}^{-1}(q) = \alpha - 2\beta_0 + U + D_{f,22}^{-1}(q), \quad (\text{A62})$$

$$D_{23}^{-1}(q) = -D_{32}^{-1}(q) = \omega_n \left[ 1 - \frac{i}{2}Z_2^{(1)}Z_3^{(1)}\Pi_1(q) \right], \quad (\text{A63})$$

$$D_{24}^{-1}(q) = D_{42}^{-1}(q) = D_{f,24}^{-1}(q), \quad (\text{A64})$$

$$D_{25}^{-1}(q) = D_{52}^{-1}(q) = -\sqrt{2}d - \frac{1}{2\sqrt{2}}z_0Z_2^{(1)}\Pi_1(q), \quad (\text{A65})$$

$$D_{26}^{-1}(q) = D_{62}^{-1}(q) = d, \quad (\text{A66})$$

$$D_{33}^{-1}(q) = \alpha - 2\beta_0 + U + z_0Z_{33}^{(2)}\xi_{\mathbf{0}} + \left| \frac{\partial z}{\partial d''} \right|^2 \left[ \xi_{\mathbf{0}} + \frac{\omega_n^2}{2z_0^2}\Pi_0(q) \right], \quad (\text{A67})$$

$$D_{34}^{-1}(q) = -D_{43}^{-1}(q) = \frac{i\omega_n}{2}Z_4^{(1)}Z_3^{(1)}\Pi_1(q), \quad (\text{A68})$$

$$D_{35}^{-1}(q) = -D_{53}^{-1}(q) = \frac{i\omega_n}{2\sqrt{2}z_0}Z_3^{(1)}\Pi_0(q), \quad (\text{A69})$$

$$D_{36}^{-1}(q) = D_{63}^{-1}(q) = 0, \quad (\text{A70})$$

$$D_{44}^{-1}(q) = V_{\mathbf{q}} + D_{f,4,4}^{-1}(q), \quad (\text{A71})$$

$$D_{45}^{-1}(q) = D_{54}^{-1}(q) = -\frac{1}{2} \left[ 1 + \frac{1}{\sqrt{2}}z_0Z_4^{(1)}\Pi_1(q) \right], \quad (\text{A72})$$

$$D_{46}^{-1}(q) = D_{64}^{-1}(q) = \frac{1}{\sqrt{2}}, \quad (\text{A73})$$

$$D_{55}^{-1}(q) = -\frac{1}{4}\Pi_0(q), \quad (\text{A74})$$

$$D_{56}^{-1}(q) = D_{65}^{-1}(q) = D_{66}^{-1}(q) = 0, \quad (\text{A75})$$

where

$$Z_{\mu}^{(1)} = Z_{\uparrow,\mu}^{(1)} = Z_{\downarrow,\mu}^{(1)}, \quad (\text{A76})$$

$$Z_{\mu\nu}^{(2)} = Z_{\uparrow,\mu\nu}^{(2)} = Z_{\downarrow,\mu\nu}^{(2)}, \quad (\text{A77})$$

$$D_{f,\mu\nu}^{-1}(q) = z_0Z_{\mu\nu}^{(2)}\xi_{\mathbf{0}} + Z_{\mu}^{(1)}Z_{\nu}^{(1)} \left( \xi_{\mathbf{q}} - \frac{1}{2}z_0^2\Pi_2(q) \right). \quad (\text{A78})$$

While, in the spin fluctuations sector, we find

$$D_{77}^{-1}(q) = z_0Z_{77}^{(2)}\xi_{\mathbf{0}} + \left( \frac{\partial z_{\uparrow}}{\partial R_z} \right)^2 \left[ \xi_{\mathbf{q}} - \frac{z_0^2}{2}\Pi_2(q) \right], \quad (\text{A79})$$

$$D_{78}^{-1}(q) = D_{87}^{-1}(q) = -\frac{1}{2} \left[ 1 + \frac{1}{\sqrt{2}}z_0\frac{\partial z_{\uparrow}}{\partial R_z}\Pi_1(q) \right], \quad (\text{A80})$$

$$D_{88}^{-1}(q) = -\frac{1}{4}\Pi_0(q), \quad (\text{A81})$$

where

$$\frac{\partial z_{\uparrow}}{\partial R_z} = \frac{\partial z_{\uparrow,i}(\tau)}{\partial R_{z,i}(\tau)} \Big|_{\psi=\psi^{\text{SP}}}. \quad (\text{A82})$$

The spin sector of the inverse propagator is identical to that computed in Ref. [47] for the Hubbard model (i.e. without long range interactions), as can be checked by expressing the derivatives of  $z_{\sigma}$  with respect to the squared radial fields in terms of their counterpart in terms of the radial fields, and using the saddle-point equations to identify occurring  $\alpha$  and  $\beta_0$  terms in the obtained expressions. In the  $V \rightarrow 0$  limit, the charge sector of the inverse propagator can also be shown to coincide with that of Ref. [47] by the same argument.

### 3. Density autocorrelation function

In this work, we are interested in the computation of the dynamical dielectric function, which itself depends on the dynamical charge susceptibility  $\chi_c(\mathbf{q}, \omega)$ . The latter may be obtained by analytical continuation of the density-density correlator

$$\chi_c(q) = \langle n(-q)n(q) \rangle = 4d^2 \langle \delta d'(-q)\delta d'(q) \rangle - 2d \langle \delta d'(-q)\delta R_e(q) \rangle + \langle \delta R_e(-q)\delta R_e(q) \rangle. \quad (\text{A83})$$

Inverting the charge sector of  $\underline{D}^{-1}(q)$ , and using the fact that the slave boson correlation functions are straightforwardly obtained as matrix elements of the propagator for the slave boson fields fluctuations

$$\langle \delta \psi_{\mu}(-q)\delta \psi_{\nu}(q) \rangle = \frac{1}{2} D_{\mu\nu}(q), \quad (\text{A84})$$

we obtain the explicit form of Eq. (A83) as:

$$\chi_c(q) = \frac{x^2 D_{55}^{-1}(q) \{s_{33}[\Delta_1(q) - 4\sqrt{2}d\Delta_2(q) + 8d^2\Delta_3(q)] + \frac{1}{4}\omega_n^2 D_{55}^{-1}(q)\}}{4s_{33}x^2[\Delta_2^2(q) - \Delta_1(q)\Delta_3(q)] - \omega_n^2 D_{55}^{-1}(q)[\frac{1}{2}\Delta_1(q) + \sqrt{2}(x-2d)\Delta_2(q) + (x-2d)^2\Delta_3(q)]}, \quad (\text{A85})$$

where

$$s_{33} = \xi_0 \left( \left| Z_3^{(1)} \right|^2 - \frac{z_0}{d} Z_2^{(1)} \right), \quad (\text{A86})$$

$$\Delta_1(q) = -D_{55}^{-1}(q) \left[ \frac{1}{4} D_{22}^{-1}(q) - dD_{12}^{-1}(q) + d^2 D_{11}^{-1}(q) \right] + \left[ \frac{1}{2} D_{25}^{-1}(q) - dD_{15}^{-1}(q) \right]^2, \quad (\text{A87})$$

$$\begin{aligned} \Delta_2(q) = & -D_{55}^{-1}(q) \left[ \frac{1}{4} D_{24}^{-1}(q) - \frac{d}{2} D_{14}^{-1}(q) - \frac{1}{2\sqrt{2}} D_{12}^{-1}(q) + \frac{d}{\sqrt{2}} D_{11}^{-1}(q) \right] \\ & + \left[ \frac{1}{2} D_{25}^{-1}(q) - dD_{15}^{-1}(q) \right] \left[ \frac{1}{2} D_{45}^{-1}(q) - \frac{1}{\sqrt{2}} D_{15}^{-1}(q) \right], \end{aligned} \quad (\text{A88})$$

$$\Delta_3(q) = -D_{55}^{-1}(q) \left[ \frac{1}{4} D_{44}^{-1}(q) - \frac{1}{\sqrt{2}} D_{1,4}^{-1}(q) + \frac{1}{2} D_{1,1}^{-1}(q) \right] + \left[ \frac{1}{2} D_{45}^{-1}(q) - \frac{1}{\sqrt{2}} D_{15}^{-1}(q) \right]^2. \quad (\text{A89})$$

#### Appendix B: Slave boson mean-field and the Landau-Fermi liquid

Note that, in the paramagnetic mean-field, the KRSB mapping of the physical electron field reduces to  $c_{\sigma,i} \rightarrow z_0 f_{\sigma,i}$ . Therefore, the electron's non-interacting Green's function  $G_{0,\sigma ij}(\tau) = -\langle \mathcal{T}_{\tau} c_{\sigma,i}(\tau) c_{\sigma,j}^*(0) \rangle$  may be straightforwardly expressed in terms of its similarly defined KRSB counterpart  $\tilde{G}_{0,\sigma ij}(\tau)$  as:

$$G_{0,\sigma ij}(\tau) = z_0^2 \tilde{G}_{0,\sigma ij}(\tau). \quad (\text{B1})$$

In terms of the polarizabilities  $\Pi_0$  and  $\Pi_0^{(0)}$ , this result translates to

$$\Pi_0(\mathbf{q}, \omega) = \frac{1}{z_0^2} \Pi_0^{(0)} \left( \mathbf{q}, \frac{\omega}{z_0} \right). \quad (\text{B2})$$

This equality is merely a re-statement, in terms of the KRSB inverse effective mass renormalization factor  $z_0^2$ , of the standard result from Landau's theory of the Fermi liquid that interactions renormalize the electron gas through the quasiparticle residue [6].

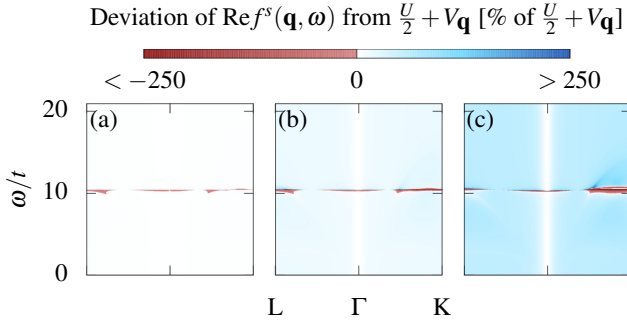


FIG. 4. Deviation of  $\text{Re}f^s(\mathbf{q}, \omega)$  from  $\frac{U}{2} + V_{\mathbf{q}}$ . Parameters:  $T = 0$ , and  $V = 0.1 U$  with (a)  $U = 0.01 U_c$ , (b)  $U = 0.10 U_c$  and (c)  $U = 0.30 U_c$ .

### Appendix C: Deviation of the radial KRSB charge susceptibility from RPA

In order to assess for the agreement, or disagreement, between the radial KRSB spectra and the predictions of standard perturbation theory, let us compute the dynamical spin-symmetric density interaction function  $f^s(\mathbf{q}, \omega)$ , defined as

$$f^s(\mathbf{q}, \omega) = \frac{1}{\chi_c(\mathbf{q}, \omega)} - \frac{1}{\Pi_0(\mathbf{q}, \omega)}. \quad (\text{C1})$$

Note that this quantity is a wavevector and frequency dependent generalization of the usual Landau parameter  $F_0^s = N(0)f^s(\mathbf{0}, 0)$ , with  $N(0)$  the density of states at the Fermi energy. Let us also observe that  $f^s$  is essentially akin to a many-body local field factor, as sometimes introduced in early attempts to provide corrections to the RPA charge susceptibility [6]. In the weak coupling regime, the real part of this function should be equal to  $\frac{U}{2} + V_{\mathbf{q}}$ , which would yield the standard RPA charge susceptibility, and deviation from this value thus give a measure of the deviation of the radial KRSB results from perturbation theory.

As can be seen in Fig. 4(a), in which this deviation is displayed, for  $V = 0.1 U$ , with  $U = 0.01 U_c$ , the radial KRSB results agree with standard perturbation theory in the weak coupling regime. Indeed, we find  $\text{Re}f^s(\mathbf{q}, \omega) \simeq \frac{U}{2} + V_{\mathbf{q}}$ , with deviations of at most 1.5%, irrespective of the energy and wavevector, except in a narrow band around  $\omega = U_c/2$ . There, deviations of up to 115% are observed. For reasons discussed in the main text, we assign this band to a signature of the upper Hubbard band (UHB), and note that strong deviations around this UHB mode are to be expected, as it is not captured by standard perturbative expansions. As the Hubbard coupling is increased, we observe in Fig. 4(b) and Fig. 4(c) that deviations from  $\text{Re}f^s(\mathbf{q}, \omega) \simeq \frac{U}{2} + V_{\mathbf{q}}$  grow, jointly with the deviations around the UHB mode.[70] In particular, we find deviations of up to 15% for  $U = 0.10 U_c$ , and 60% for  $U = 0.30 U_c$ , outside of the UHB. Additionally the dispersion of the latter is also seen to increase, due to the larger values of  $U = 0.10 U_c$  and  $0.30 U_c$  in Fig. 4(b) and Fig. 4(c), respectively.

### Appendix D: Plasma frequency on a lattice in the weak coupling regime

The dispersion  $\omega_{\text{plasmon}}(\mathbf{q})$  of the plasmon collective mode is obtained as a solution of

$$\varepsilon(\mathbf{q}, \omega_{\text{plasmon}}(\mathbf{q})) = 0. \quad (\text{D1})$$

In the weak coupling regime  $U \ll U_c$  and  $V \ll U_c$ , an analytical expression for the leading contributions to the plasmon dispersion may be obtained by noting that the radial KRSB dielectric function reduces to an RPA form

$$\varepsilon(\mathbf{q}, \omega) \simeq 1 + \left( \frac{U}{2} + V_{\mathbf{q}} \right) \Pi_0(\mathbf{q}, \omega). \quad (\text{D2})$$

For our purpose, we expand the Lindhard function to lowest order in  $\mathbf{q}^2$  about  $\mathbf{q} = \Gamma$ . Re-writing it as

$$\Pi_0(\mathbf{q}, \omega) = \frac{2}{L} \sum_{\mathbf{k}} \frac{n_F(E_{\mathbf{k}+\mathbf{q}}) - n_F(E_{\mathbf{k}})}{\omega - (E_{\mathbf{k}+\mathbf{q}} - E_{\mathbf{k}})} = \frac{2}{L} \sum_{\mathbf{k}} n_F(E_{\mathbf{k}}) \frac{2E_{\mathbf{k}} - E_{\mathbf{k}+\mathbf{q}} - E_{\mathbf{k}-\mathbf{q}}}{\omega^2 + \omega(E_{\mathbf{k}-\mathbf{q}} - E_{\mathbf{k}+\mathbf{q}}) + (E_{\mathbf{k}+\mathbf{q}} - E_{\mathbf{k}})(E_{\mathbf{k}} - E_{\mathbf{k}-\mathbf{q}})}, \quad (\text{D3})$$

then expanding the dispersion as  $E_{\mathbf{k}\pm\mathbf{q}} = E_{\mathbf{k}} \pm \mathbf{q}^T \nabla_{\mathbf{k}} E_{\mathbf{k}} + \frac{1}{2} \mathbf{q}^T \mathbf{H}(E_{\mathbf{k}}) \mathbf{q} + O(q^3)$ , with  $\mathbf{H}(E_{\mathbf{k}})$  the Hessian matrix  $H_{ab}(E_{\mathbf{k}}) = \partial^2 E_{\mathbf{k}} / \partial k_a \partial k_b$ , and using  $\omega \gg |\mathbf{q}| \equiv q$  (since  $\omega_p$  remains finite for finite  $V$ ), we find

$$\Pi_0(\mathbf{q}, \omega) \simeq -\frac{2}{L} \sum_{\mathbf{k}} n_F(E_{\mathbf{k}}) \frac{\mathbf{q}^T \mathbf{H}(E_{\mathbf{k}}) \mathbf{q}}{\omega^2}. \quad (\text{D4})$$

We can moreover make use of the fact that the off-diagonal matrix elements of the Hessian are odd with respect to the components of  $\mathbf{k}$ , as well as the invariance of the remaining integrals under permutations of the in-

dices of  $\mathbf{H}$ , such that we end up with the simple form

$$\begin{aligned}\Pi_0(\mathbf{q}, \omega) &= -\frac{2}{L} \sum_{\mathbf{k}} n_F(E_{\mathbf{k}}) \frac{\sum_a q_a^2 H_{aa}(E_{\mathbf{k}})}{\omega^2} \\ &= -\frac{q^2}{\omega^2} \frac{2t}{L} \sum_{\mathbf{k}} n_F(E_{\mathbf{k}}) \cos \frac{k_x}{2} \left( \cos \frac{k_y}{2} + \cos \frac{k_z}{2} \right) \\ &= \frac{q^2}{\omega^2} \frac{\xi_0}{6},\end{aligned}\quad (\text{D5})$$

where  $\xi_0$  is the bare average kinetic energy per lattice site. Inserting this expression into Eq. (D2), we finally find

$$\omega_{\text{plasmon}}^2(\mathbf{q}) \simeq \omega_p^2 + \kappa q^2, \quad (\text{D6})$$

with

$$\omega_p^2 = -\frac{V\xi_0}{6}, \quad (\text{D7})$$

and

$$\kappa = -\frac{U\xi_0}{12}. \quad (\text{D8})$$

$V$  is hence pivotal to the very existence of the plasmon altogether, while  $U$  rather governs its dispersion. Moreover, both  $\omega_p$  and  $\kappa$  are sensitive to the lattice on which the electrons evolve through the  $-\xi_0/6$  factor. Finally,

recalling that in free space  $V = e^2$ , and that the kinetic energy is proportional to the inverse band mass via  $t \sim 1/m^*$ , we may thus rewrite  $\xi_0 \sim -6 \varrho/m^*$ , with

$$\begin{aligned}\varrho &\equiv \frac{2}{Lt} \sum_{\mathbf{k}} n_F(E_{\mathbf{k}}) \frac{\partial^2 E_{\mathbf{k}}}{\partial k_x^2} \\ &= \frac{2}{L} \sum_{\mathbf{k}} n_F(E_{\mathbf{k}}) \cos \frac{k_x}{2} \left( \cos \frac{k_y}{2} + \cos \frac{k_z}{2} \right).\end{aligned}\quad (\text{D9})$$

The plasma frequency is then recast as

$$\omega_p = \sqrt{\frac{4\pi e^2 \varrho}{m^*}}. \quad (\text{D10})$$

This is the classical expression, apart from the fact that the electron density  $n$  has been replaced by  $\varrho$ . The difference stems from the way we represent the density distribution on the lattice. In contrast to the Fermi gas, for which a homogeneous electron density is given by a continuous (constant in this case) function of the position, we here deal with a discretized and periodic function of the position  $\mathbf{R}$ :  $n(\mathbf{R}) \sim \sum_j \delta(\mathbf{R} - \mathbf{r}_j)$ , where  $\mathbf{r}_j$  is a lattice vector. The Coulomb potential then couples to this set of discrete and periodic lattice bonds, and taking its Fourier transform results in contributions from the lattice harmonics. Therefore, the lattice-dependent  $\varrho$  appears in the plasma frequency instead of  $n = 2 \int \frac{d^3 \mathbf{p}}{(2\pi)^3} n_F(\frac{p^2}{2m^*})$  for the Fermi gas.

- 
- [1] D. Bohm and D. Pines, A collective description of electron interactions. I. magnetic interactions, *Phys. Rev.* **82**, 625 (1951).
- [2] D. Pines and D. Bohm, A collective description of electron interactions: II. collective vs individual particle aspects of the interactions, *Phys. Rev.* **85**, 338 (1952).
- [3] D. Bohm and D. Pines, A collective description of electron interactions: III. coulomb interactions in a degenerate electron gas, *Phys. Rev.* **92**, 609 (1953).
- [4] P. W. Anderson, *Basic Notions of Condensed Matter Physics* (Addison-Wesley, Redwood City, CA, 1994).
- [5] J. R. Schrieffer, *Theory of Superconductivity* (Frontiers in Physics, Addison-Wesley, New York, NY, 1964).
- [6] G. Giuliani and G. Vignale, *Quantum Theory of the Electron Liquid* (Cambridge University Press, 2005).
- [7] W. Yan and N. A. Mortensen, Nonclassical effects in plasmonics: An energy perspective to quantify nonclassical effects, *Phys. Rev. B* **93**, 115439 (2016).
- [8] D. E. Chang, A. S. Sørensen, E. A. Demler, and M. D. Lukin, A single-photon transistor using nanoscale surface plasmons, *Nat. Phys.* **3**, 807 (2007).
- [9] H. J. Lezec, J. A. Dionne, and H. A. Atwater, Negative refraction at visible frequencies, *Science* **316**, 430 (2007).
- [10] A. V. Akimov, A. Mukherjee, C. L. Yu, D. E. Chang, A. S. Zibrov, P. R. Hemmer, H. Park, and M. D. Lukin, Generation of single optical plasmons in metallic nanowires coupled to quantum dots, *Nature* **450**, 402 (2007).
- [11] M. A. Noginov, G. Zhu, A. M. Belgrave, R. Bakker, V. M. Shalaev, E. E. Narimanov, S. Stout, E. Herz, T. Suteewong, and U. Wiesner, Demonstration of a spaser-based nanolaser, *Nature* **460**, 1110 (2009).
- [12] R. F. Oulton, V. J. Sorger, T. Zentgraf, R.-M. Ma, C. Gladden, L. Dai, G. Bartal, and X. Zhang, Plasmon lasers at deep subwavelength scale, *Nature* **461**, 629 (2009).
- [13] W. Cai, J. S. White, and M. L. Brongersma, Compact, high-speed and power-efficient electrooptic plasmonic modulators, *Nano Lett.* **9**, 4403 (2009).
- [14] A. Hryciw, Y. C. Jun, and M. L. Brongersma, Electrifying plasmonics on silicon, *Nat. Mater.* **9**, 3 (2010).
- [15] J. A. Schuller, E. S. Barnard, W. Cai, Y. C. Jun, J. S. White, and M. L. Brongersma, Plasmonics for extreme light concentration and manipulation, *Nat. Mater.* **9**, 193 (2010).
- [16] T. Ergin, N. Stenger, P. Brenner, J. B. Pendry, and M. Wegener, Three-dimensional invisibility cloak at optical wavelengths, *Science* **328**, 337 (2010).
- [17] K. M. Mayer and J. H. Hafner, Localized surface plasmon resonance sensors, *Chem. Rev.* **111**, 3828 (2011).
- [18] A. Boltasseva and H. A. Atwater, Low-loss plasmonic metamaterials, *Science* **331**, 290 (2011).
- [19] C. M. Soukoulis and M. Wegener, Past achievements and future challenges in the development of three-dimensional photonic metamaterials, *Nat. Photon.* **5**, 523 (2011).
- [20] K. C. Y. Huang, M.-K. Seo, T. Sarmiento, Y. Huo,

- J. S. Harris, and M. L. Brongersma, Electrically driven subwavelength optical nanocircuits, *Nat. Photon.* **8**, 244 (2014).
- [21] A. Baev, P. N. Prasad, H. Ågren, M. Samoć, and M. Wegener, Metaphotonics: An emerging field with opportunities and challenges, *Phys. Rep.* **594**, 1 (2015).
- [22] H. A. Atwater and A. Polman, Plasmonics for improved photovoltaic devices, *Nat. Mater.* **9**, 205 (2010).
- [23] S. Linic, P. Christopher, and D. B. Ingram, Plasmonic-metal nanostructures for efficient conversion of solar to chemical energy, *Nat. Mater.* **10**, 911 (2011).
- [24] W. Hou, W. H. Hung, P. Pavaskar, A. Goepfert, M. Aykol, and S. B. Cronin, Photocatalytic conversion of CO<sub>2</sub> to hydrocarbon fuels via plasmon-enhanced absorption and metallic interband transitions, *ACS Catal.* **1**, 929 (2011).
- [25] J. Lee, S. Mubeen, X. Ji, G. D. Stucky, and M. Moskovits, Plasmonic photoanodes for solar water splitting with visible light, *Nano Lett.* **12**, 5014 (2012).
- [26] S. Mukherjee, F. Libisch, N. Large, O. Neumann, L. V. Brown, J. Cheng, J. B. Lassiter, E. A. Carter, P. Nordlander, and N. J. Halas, Hot electrons do the impossible: Plasmon-induced dissociation of H<sub>2</sub> on Au, *Nano Lett.* **13**, 240 (2013).
- [27] D. O’Neal, L. R. Hirsch, N. J. Halas, J. Payne, and J. L. West, Photo-thermal tumor ablation in mice using near infrared-absorbing nanoparticles, *Cancer Lett.* **209**, 171 (2004).
- [28] Y. Li, C. Jing, L. Zhang, and Y.-T. Long, Resonance scattering particles as biological nanosensors in vitro and in vivo, *Chem. Soc. Rev.* **41**, 632 (2012).
- [29] M. Swierczewska, G. Liu, S. Lee, and X. Chen, High-sensitivity nanosensors for biomarker detection, *Chem. Soc. Rev.* **41**, 2641 (2012).
- [30] C. L. C. Smith, N. Stenger, A. Kristensen, N. A. Mortensen, and S. I. Bozhevolnyi, Gap and channeled plasmons in tapered grooves: a review, *Nanoscale* **7**, 9355 (2015).
- [31] V. P. Chavda, P. C. Balar, L. V. Nalla, R. Bezbaruah, N. R. Gogoi, S. N. R. Gajula, B. Peng, A. S. Meena, J. Conde, and R. Prasad, Conjugated nanoparticles for solid tumor theranostics: Unraveling the interplay of known and unknown factors, *ACS Omega* **8**, 37654 (2023).
- [32] A. M. Lewis and T. C. Berkelbach, Ab initio lifetime and concomitant double-excitation character of plasmons at metallic densities, *Phys. Rev. Lett.* **122**, 226402 (2019).
- [33] P. Li, R. Shi, P. Lin, and X. Ren, First-principles calculations of plasmon excitations in graphene, silicene, and germanene, *Phys. Rev. B* **107**, 035433 (2023).
- [34] C. J. C. Scott and G. H. Booth, Rigorous screened interactions for realistic correlated electron systems, *Phys. Rev. Lett.* **132**, 076401 (2024).
- [35] E. G. C. P. van Loon, H. Hafermann, A. I. Lichtenstein, A. N. Rubtsov, and M. I. Katsnelson, Plasmons in strongly correlated systems: Spectral weight transfer and renormalized dispersion, *Phys. Rev. Lett.* **113**, 246407 (2014).
- [36] H. Hafermann, E. G. C. P. van Loon, M. I. Katsnelson, A. I. Lichtenstein, and O. Parcollet, Collective charge excitations of strongly correlated electrons, vertex corrections, and gauge invariance, *Phys. Rev. B* **90**, 235105 (2014).
- [37] M. Guzzo, G. Lani, F. Sottile, P. Romaniello, M. Gatti, J. J. Kas, J. J. Rehr, M. G. Silly, F. Sirotti, and L. Reining, Valence electron photoemission spectrum of semiconductors: Ab initio description of multiple satellites, *Phys. Rev. Lett.* **107**, 166401 (2011).
- [38] J. S. Zhou, M. Gatti, J. J. Kas, J. J. Rehr, and L. Reining, Cumulant Green’s function calculations of plasmon satellites in bulk sodium: Influence of screening and the crystal environment, *Phys. Rev. B* **97**, 035137 (2018).
- [39] P. Cudazzo and L. Reining, Correlation satellites in optical and loss spectra, *Phys. Rev. Res.* **2**, 012032(R) (2020).
- [40] L. Zinni, M. Bejas, H. Yamase, and A. Greco, Low-energy plasmon excitations in infinite-layer nickelates, *Phys. Rev. B* **107**, 014503 (2023).
- [41] G. Kotliar and A. E. Ruckenstein, New functional integral approach to strongly correlated Fermi systems: The Gutzwiller approximation as a saddle point, *Phys. Rev. Lett.* **57**, 1362 (1986).
- [42] M. Deeg, H. Fehske, and H. Büttner, Slave-boson phase diagram of the two-dimensional extended Hubbard model: Influence of electron-phonon coupling, *Z. Phys. B* **91** (1993).
- [43] G. Lhoutellier, R. Frésard, and A. M. Oleś, Fermi-liquid Landau parameters for a nondegenerate band: Spin and charge instabilities in the extended Hubbard model, *Phys. Rev. B* **91**, 224410 (2015).
- [44] D. Riegler, J. Seufert, E. H. da Silva Neto, P. Wölfle, R. Thomale, and M. Klett, Interplay of spin and charge order in the electron-doped cuprates, *Phys. Rev. B* **108**, 195141 (2023).
- [45] L. Philoxene, V. H. Dao, and R. Frésard, Spin and charge modulations of a half-filled extended Hubbard model, *Phys. Rev. B* **106**, 235131 (2022).
- [46] In particular, the paramagnetic saddle-point approximation of the KRMB representation is equivalent to the Gutzwiller approximation, thereby describing the MIT at half filling. On the cubic lattice, the MIT critical coupling  $U_c = 1.33W$  [43], where  $W$  is the bare bandwidth, compares favorably with the DMFT result of  $U_c = 1.17W$  [71].
- [47] V. H. Dao and R. Frésard, Collective modes in the paramagnetic phase of the Hubbard model, *Phys. Rev. B* **95**, 165127 (2017).
- [48] M. Aichhorn, H. G. Evertz, W. von der Linden, and M. Potthoff, Charge ordering in extended Hubbard models: Variational cluster approach, *Phys. Rev. B* **70**, 235107 (2004).
- [49] B. Davoudi and A.-M. S. Tremblay, Nearest-neighbor repulsion and competing charge and spin order in the extended Hubbard model, *Phys. Rev. B* **74**, 035113 (2006).
- [50] M. Y. Kagan, D. V. Efremov, M. S. Marienko, and V. V. Val’kov, Triplet p-wave superconductivity in the low-density extended Hubbard model with Coulomb repulsion, *JETP Lett.* **93**, 725 (2011).
- [51] T. Ayral, S. Biermann, and P. Werner, Screening and nonlocal correlations in the extended Hubbard model from self-consistent combined  $GW$  and dynamical mean field theory, *Phys. Rev. B* **87**, 125149 (2013).
- [52] E. G. C. P. van Loon, A. I. Lichtenstein, M. I. Katsnelson, O. Parcollet, and H. Hafermann, Beyond extended dynamical mean-field theory: Dual boson approach to the two-dimensional extended Hubbard model, *Phys. Rev. B* **90**, 235135 (2014).
- [53] K. J. Kapcia, S. Robaszkiewicz, M. Capone, and A. Amaricci, Doping-driven metal-insulator transitions



- and charge orderings in the extended Hubbard model, Phys. Rev. B **95**, 125112 (2017).
- [54] M. Schüler, E. G. C. P. van Loon, M. I. Katsnelson, and T. O. Wehling, First-order metal-insulator transitions in the extended Hubbard model due to self-consistent screening of the effective interaction, Phys. Rev. B **97**, 165135 (2018).
- [55] H. Terletska, S. Isakov, T. Maier, and E. Gull, Dynamical cluster approximation study of electron localization in the extended Hubbard model, Phys. Rev. B **104**, 085129 (2021).
- [56] M. Roig, A. T. Rømer, P. J. Hirschfeld, and B. M. Andersen, Revisiting superconductivity in the extended one-band Hubbard model: Pairing via spin and charge fluctuations, Phys. Rev. B **106**, 214530 (2022).
- [57] E. Linnér, A. I. Lichtenstein, S. Biermann, and E. A. Stepanov, Multichannel fluctuating field approach to competing instabilities in interacting electronic systems, Phys. Rev. B **108**, 035143 (2023).
- [58] S. Kundu and D. Sénéchal, CDMFT+HFD: An extension of dynamical mean field theory for nonlocal interactions applied to the single band extended Hubbard model, SciPost Phys. Core **7**, 033 (2024).
- [59] R. Frésard and T. Kopp, Slave bosons in radial gauge: the correct functional integral representation and inclusion of non-local interactions, Nucl. Phys. B **594**, 769 (2001).
- [60] V. H. Dao and R. Frésard, Combining complex and radial slave boson fields within the Kotliar-Ruckenstein representation of correlated impurities, Ann. Phys. (Berlin) **532**, 1900491 (2020).
- [61] V. H. Dao and R. Frésard, Exact functional integration of radial and complex slave-boson fields: Thermodynamics and dynamics of the two-site extended Hubbard model, Ann. Phys. (Berlin) **536**, 2400029 (2024).
- [62] T. Jolicoeur and J. C. Le Guillou, Fluctuations beyond the Gutzwiller approximation in the slave-boson approach, Phys. Rev. B **44**, 2403 (1991).
- [63] R. Frésard and P. Wölfle, Unified slave boson representation of spin and charge degrees of freedom for strongly correlated Fermi systems, Int. J. Mod. Phys. B **06**, 685 (1992).
- [64] Y. Bang, C. Castellani, M. Grilli, G. Kotliar, R. Raimondi, and Z. Wang, Single particle and optical gaps in charge-transfer insulators, Int. J. Mod. Phys. B **06**, 531 (1992).
- [65] J. Bünemann, M. Capone, J. Lorenzana, and G. Seibold, Linear-response dynamics from the time-dependent Gutzwiller approximation, New J. Phys. **15**, 053050 (2013).
- [66] K. Noatschk, C. Martens, and G. Seibold, Time-dependent Gutzwiller approximation: Theory and applications, J. Supercond. Nov. Mag. **33**, 2389 (2020).
- [67] D. Vollhardt, P. Wölfle, and P. W. Anderson, Gutzwiller-Hubbard lattice-gas model with variable density: Application to normal liquid  $^3\text{He}$ , Phys. Rev. B **35**, 6703 (1987).
- [68] R. Bulla, Zero temperature metal-insulator transition in the infinite-dimensional hubbard model, Phys. Rev. Lett. **83**, 136 (1999).
- [69] W. Zimmermann, R. Frésard, and P. Wölfle, Spin and charge structure factor of the two-dimensional Hubbard model, Phys. Rev. B **56**, 10097 (1997).
- [70] Note that, around  $\Gamma$ , the deviations of  $f^s(\mathbf{q}, \omega)$  from  $\frac{U}{2} + V_{\mathbf{q}}$  appear to vanish. This is, however, a graphical artifact which results from the divergence of  $V_{\mathbf{q}}$  at  $\Gamma$ , as the data is expressed in percents of  $\frac{U}{2} + V_{\mathbf{q}}$ .
- [71] R. Žitko, J. Bonča, and T. Pruschke, Van hove singularities in the paramagnetic phase of the hubbard model: Dmft study, Phys. Rev. B **80**, 245112 (2009).